Supplementary Information

The Ambient- and High-Temperature Oxidation Behaviour of $U^{3+}N$ and $Ln^{3+}N$ Compounds Relevant to Spent Nuclear Fuel

Pascal Uhlemann,[1]* Emily Reynolds,[2] Martina Klinkenberg,[1] Damien Prieur,[3, 4] Christian Schreinemachers,[1] Philip Kegler,[1] Celina Erven,[1] Sven M. Schenk,[2] Joerg Göttlicher,[5] Ralf Steininger,[5] Mary Blankenship,[2, 5, 6] Lothar Weinhardt,[5, 6, 7] Nina Huittinen,[3, 8] Peter Höhn,[9] Tonya Vitova,[2] Giuseppe Modolo,[1] and Gabriel. L. Murphy[1]*

[1] *Institute of Fusion Energy and Nuclear Waste Management (IFN-2), Forschungszentrum Jülich GmbH, 52428, Jülich, Germany*

[2] *Institute for Nuclear Waste Disposal (INE), Karlsruhe Institute of Technology, 76021 Karlsruhe, Germany*

[3] *Institute of Resource Ecology, Helmholtz Zentrum Dresden-Rossendorf, 01328 Dresden, Germany*

[4] *The Rossendorf Beamline at ESRF, The European Synchrotron, CS40220, 38043, Grenoble Cedex 9, France*

[5] *Institute for Photon Science and Synchrotron Radiation (IPS), Karlsruhe Institute of Technology (KIT), 76131 Karlsruhe, Germany*

[6] *Institute for Chemical Technology and Polymer Chemistry (ITCP), Karlsruhe Institute of Technology (KIT), 76131 Karlsruhe, Germany*

[7] *Department of Chemistry and Biochemistry, University of Nevada, Las Vegas (UNLV), NV 89154-4003, USA*

[8] *Institute of Chemistry and Biochemistry, Freie Universität Berlin, 14195 Berlin, Germany*

[9] *Max-Planck-Institute for Chemical Physics of Solids, 01187 Dresden, Germany*

*corresponding authors: P. Uhlemann (p.uhlemann@fz-juelich.de) and G. L. Murphy (g.murphy@fz-juelich.de)

Supplementary Information Note 1 – Isothermal Gravimetric Analysis

Supplementary Figure 1 display regression analyses performed on the weights collected during the first 10 minutes of air exposure when oxidising *Ln*N (*Ln* = Pr, Nd, Gd, Tb, Dy, Ho, Tm, Lu) and UN with less than 100 μm particle size. Table S1 summarises the regression data received.

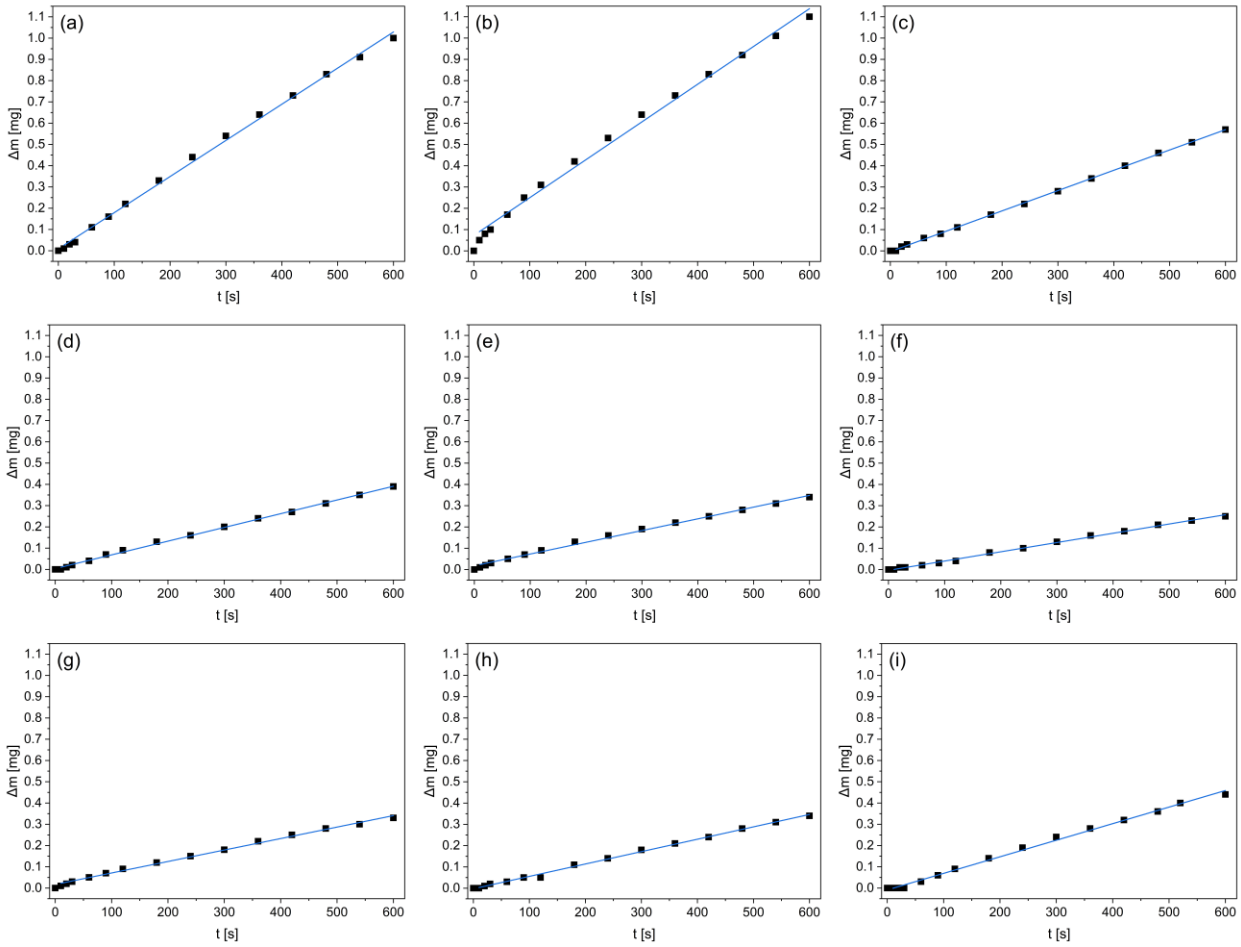

Figure S1. Applied linear regression on weights collected for 10 minutes from start of exposure of *Ln*N (*Ln* = Pr(a), Nd(b), Gd(c), Tb(d), Dy(e), Ho(f), Tm(g), Lu(h)) and UN (i) powders less than 100 μm particle size to air.

Table S1. Summary of linear regression slope, intercept and standard error of slope for the air oxidation of *Ln*N (*Ln* = Pr, Nd, Gd, Tb, Dy, Ho, Tm, Lu) and UN powders less than 100 μm particle size and their respective mass of the sample and calculated oxidation rate for 10 minutes of oxidation with 2σ uncertainty.

Compound	Slope · 10^{-4} [mg/s]	σ_{slope} · 10^{-4} [mg/s]	Intercept [mg]	m_{sample} [mg]	$\nu_{10\ min}$ [μg min^{-1}]
PrN	17.0	0.236	0.009	28.5	102.00(28)
NdN	17.8	0.379	0.072	29.2	106.80(46)
GdN	9.54	0.056	-0.003	29.4	57.30(7)
TbN	6.45	0.085	0.004	29.0	38.70(10)
DyN	5.51	0.107	0.018	30.5	33.10(13)
HoN	4.35	0.068	-0.004	28.5	26.10(8)
TmN	5.39	0.102	0.017	33.0	32.40(12)
LuN	5.82	0.091	-0.003	32.7	34.90(11)
UN	7.79	0.140	-0.009	18.6	46.80(17)

Supplementary Information Note 2 – Rietveld refinement parameters

Supplementary Table S2 summarises additional refinement details received by the performed Rietveld analysis using GSAS-II against the main compounds determined by PXRD measurements used in this work.

Table S2. Summary of additional refinement results received by GSAS-II software used to perform Rietveld refinements in this work.

Phase	$R_{w\text{-}bkg}$ [%]	$R_{w,min}$ [%]	GOF
Pristine Nitride Phases, see Table 1			
PrN	4.98	4.25	1.08
NdN	4.45	4.35	1.05
GdN	4.21	1.69	2.80
TbN	3.58	3.64	0.88
DyN	2.40	1.23	1.58
HoN	3.31	1.41	3.07
TmN	2.92	1.40	3.08
LuN	5.71	1.72	2.38
UN	2.02	1.03	1.61
Room Temperature Oxidised Phases, see Table 2			
$Pr(OH)_3$	2.29	0.77	2.28
$Nd(OH)_3$	2.20	0.85	1.88
UO_2 / U_2N_3	3.21	1.06	3.85
High Temperature Oxidised Phases, see Table S2			
$PrO_{1.82}$ / $PrO_{1.98}$	2.51	1.17	2.58
Nd_2O_3	2.57	1.27	2.62
Gd_2O_3	1.11	0.90	1.54
$TbO_{1.81}$	2.33	1.91	2.71
Dy_2O_3	1.08	0.54	2.22
Ho_2N_3	2.48	0.96	3.95
Tm_2O_3	2.53	0.73	5.83

Lu_2O_3	2.26	0.90	4.41
U_3O_8	5.60	0.87	6.57

Supplementary Information Note 3 – SEM-EDS results

Supplementary Figures S2 to S8 display the EDS results of single spot measurements on the surface of *Ln*N (*Ln* = Pr, Nd, Gd, Tb, Ho, Tm, Lu) after exposed to air and oxidised to *Ln*$(OH)_3$. Supplementary Figure S9 shows a BSE image of five different EDS spot measurements performed on the air oxidised UN, which results are summarised in the supplementary figures S10.

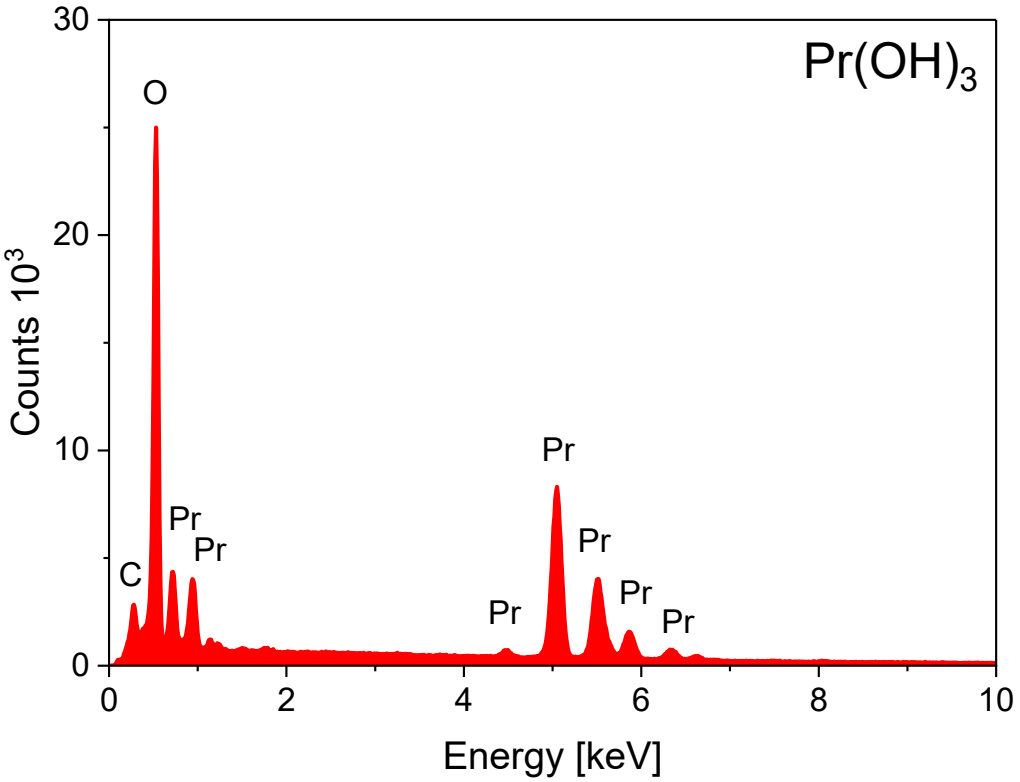

Figure S2. EDS spectrum of spot measurements on in air oxidised PrN powder, showing the complete conversion of PrN to oxidised compound.

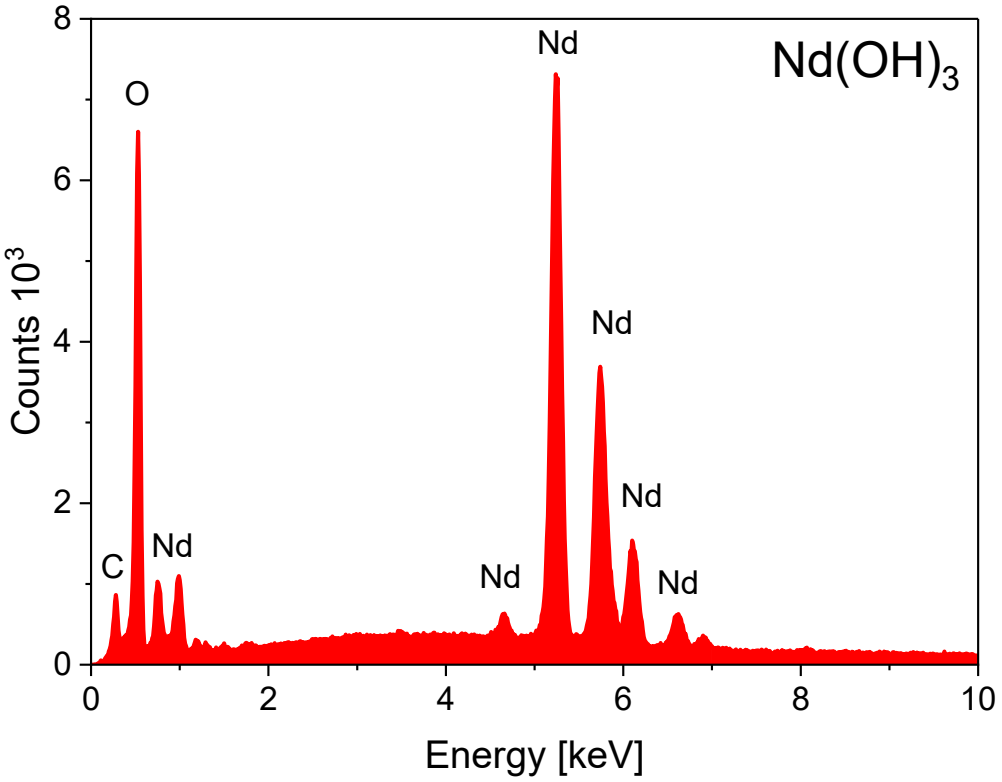

Figure S3. EDS spectrum of spot measurements on in air oxidised NdN powder, showing the complete conversion of NdN to oxidised compound.

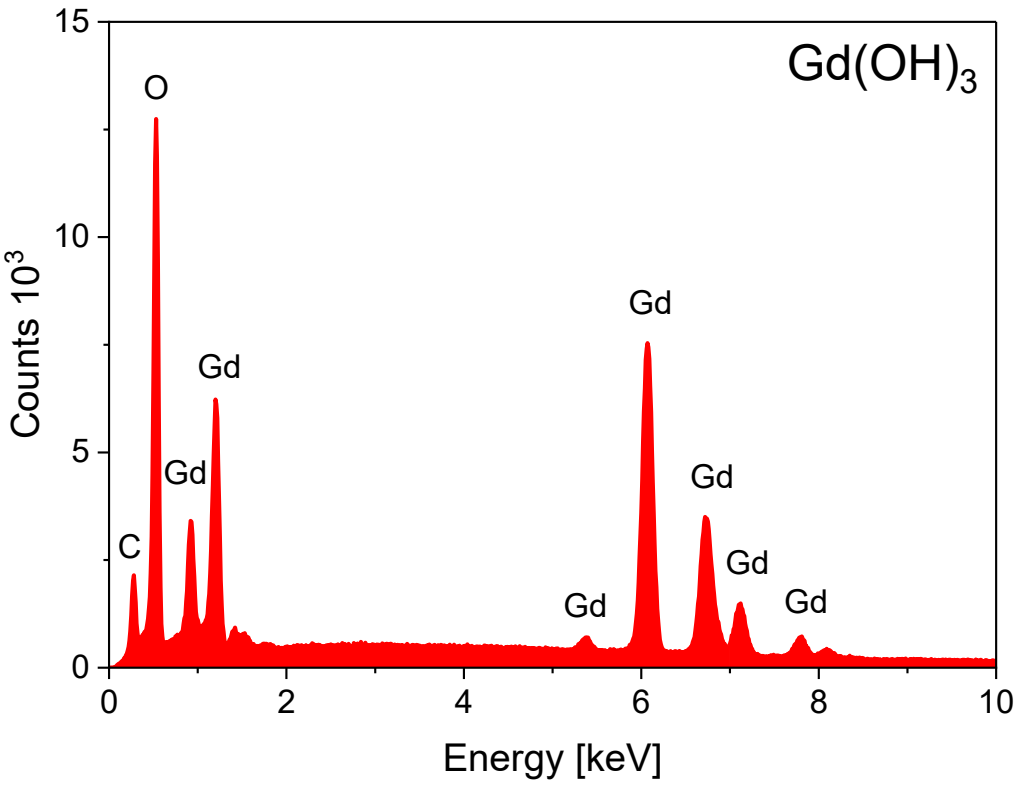

Figure S4. EDS spectrum of spot measurements on in air oxidised GdN powder, showing the complete conversion of GdN to oxidised compound.

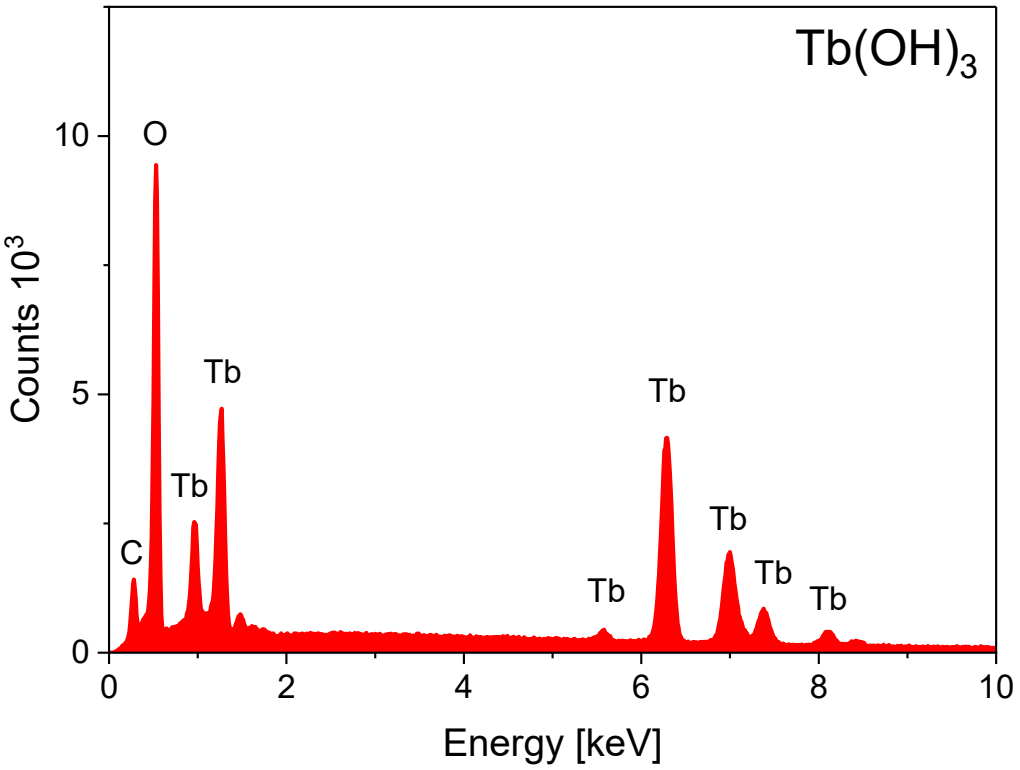

Figure S5. EDS spectrum of spot measurements on in air oxidised TbN powder, showing the complete conversion of TbN to oxidised compound.

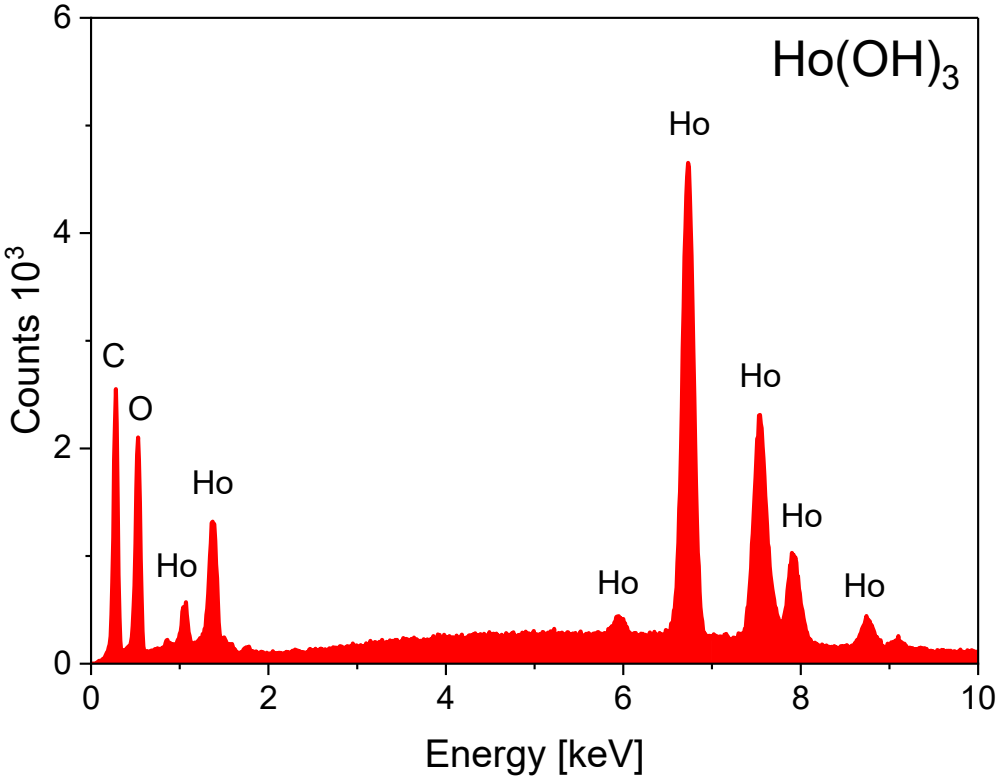

Figure S6. EDS spectrum of spot measurements on in air oxidised HoN powder, showing the complete conversion of HoN to oxidised compound.

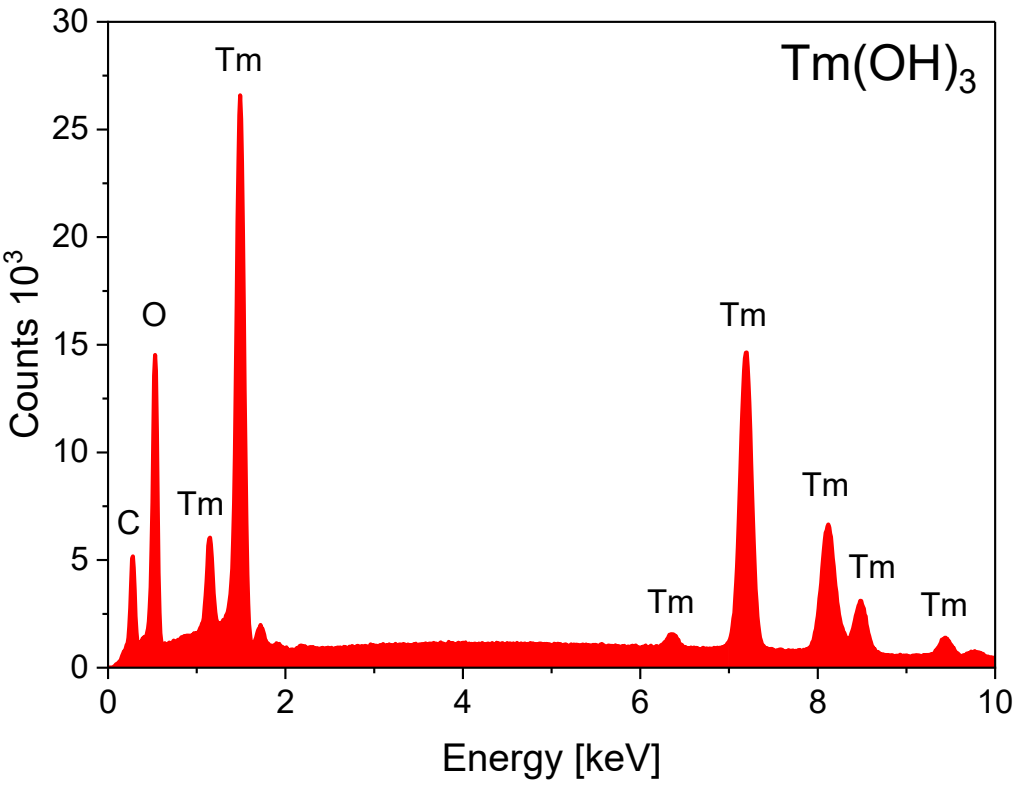

Figure S7. EDS spectrum of spot measurements on in air oxidised TmN powder, showing the complete conversion of TmN to oxidised compound.

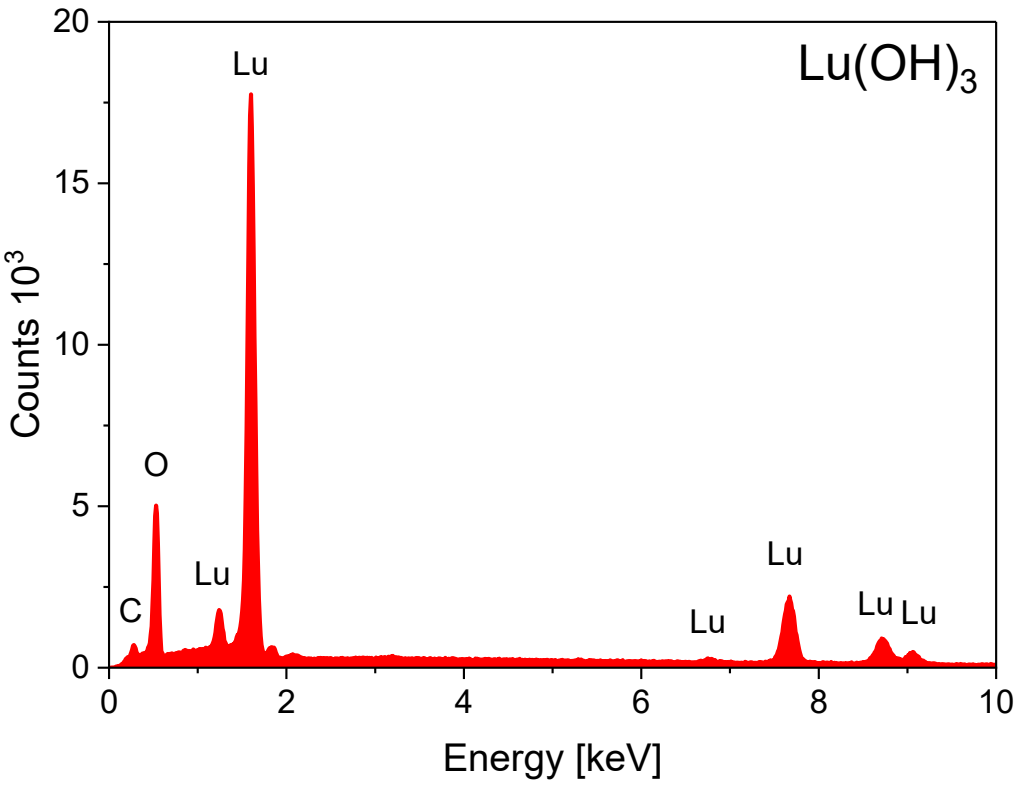

Figure S8. EDS spectrum of spot measurements on in air oxidised LuN powder, showing the complete conversion of LuN to oxidised compound.

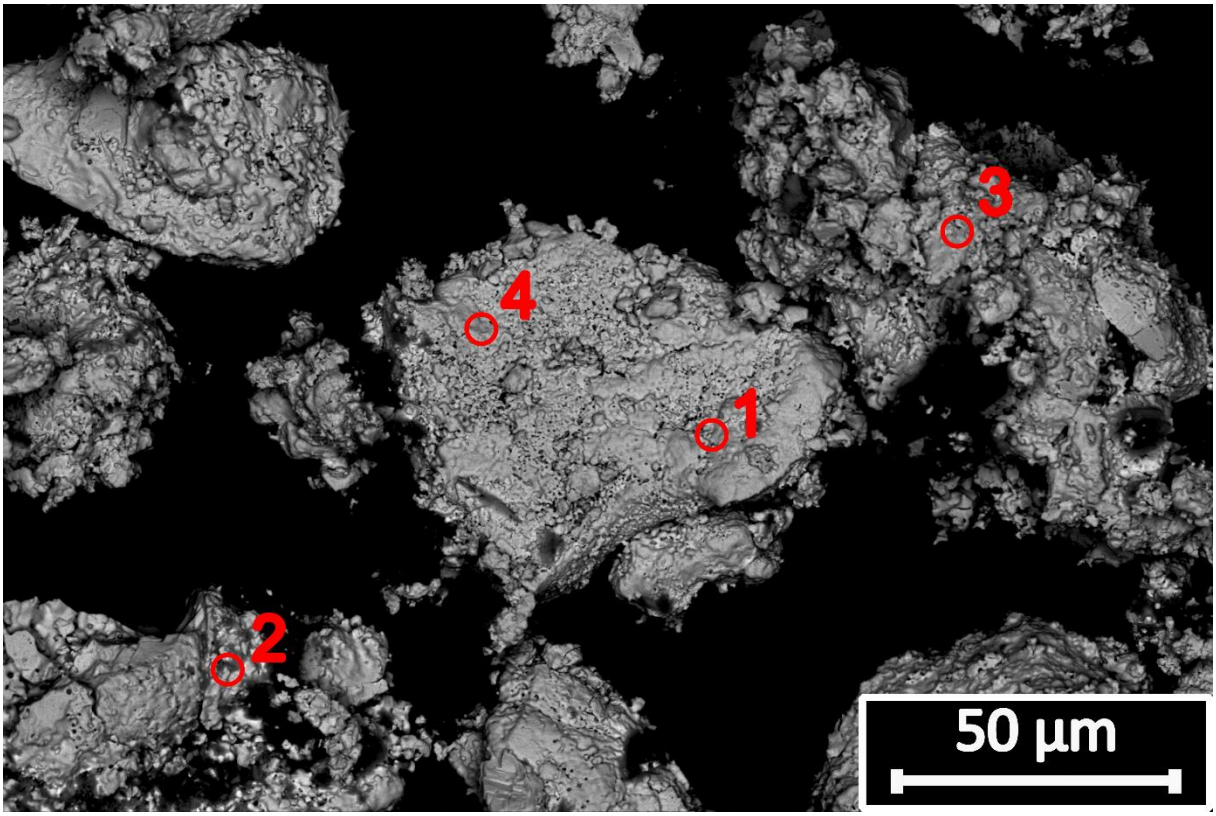

Figure S9. BSE image of room temperature oxidised UN with highlighted spots used for EDS spot measurements. An overview of the obtained spectra is given in supplementary figure S10.

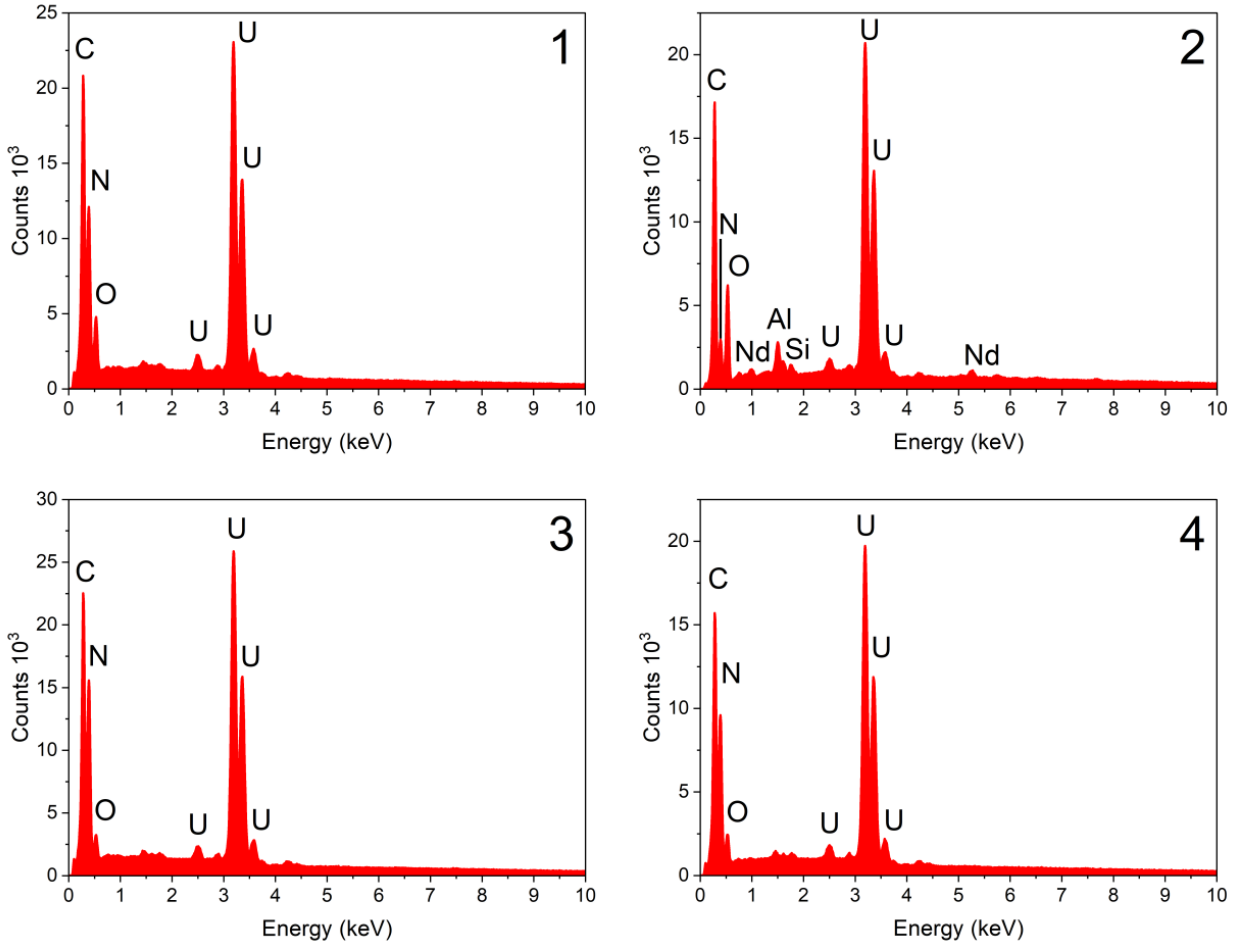

Figure S10. EDS results of spot measurements on in air oxidised UN powder, showing the incomplete oxidation of UN to UO_2/U_2N_3.

Supplementary Information Note 4 – XANES

Supplementary Figures S11 to S12 display the Rietveld profiles of UN samples with 6.4 wt%/1.5 wt% UO_2/U_2N_3 and 38.8 wt%/1.2 wt% UO_2/U_2N_3, which were used for XANES measurements.

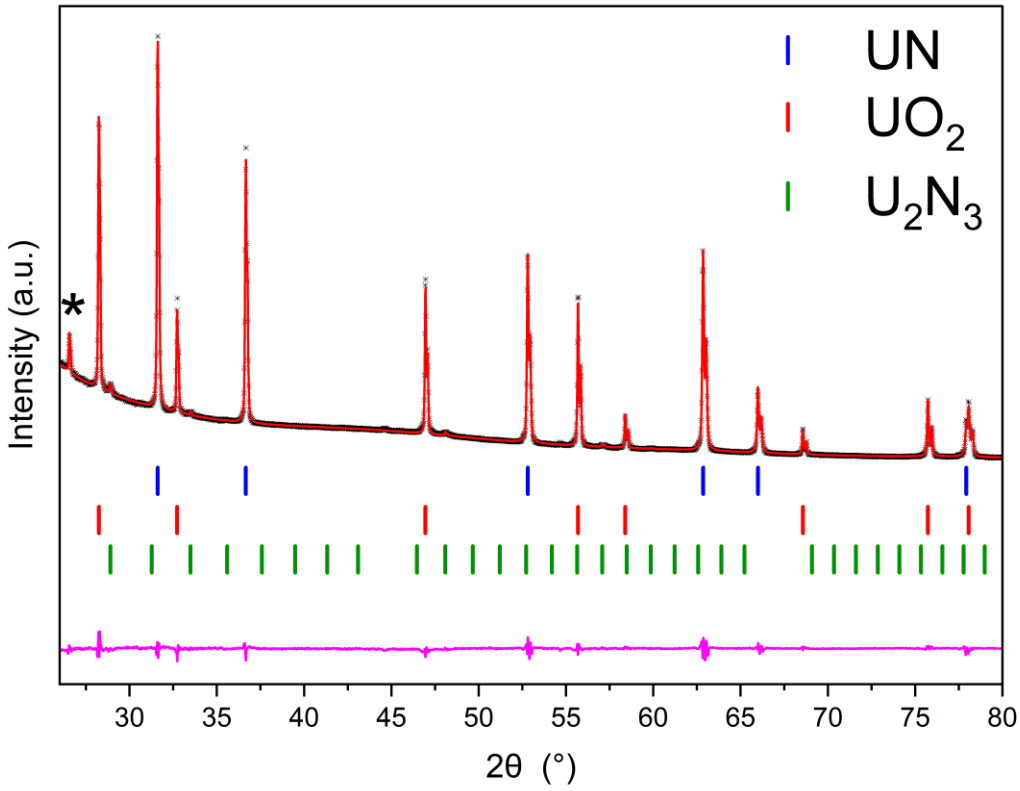

Figure S11. Rietveld profile of UN sample containing 38.8 wt% UO_2 and 1.5 wt% U_2N_3 used for XANES analysis. The black crosses, red and pink lines and vertical blue, red and violet markers respectively represent observed data, calculated profile, difference profile and allowed reflections of UN and UO_2 crystallising in cubic $Fm\bar{3}m$ structure with a = 4.900576(19) Å and a = 5.741043(24) Å respectively, U_2N_3 crystallising in $Ia\bar{3}$ structure with a = 10.698(1) Å, as well as SiO_2-phases resulting from the used Si-PXRD sample holder. The fitting parameters are R = 1.71%, R_w = 2.47%, $R_{w\text{-}bkg}$ = 2.47%, $R_{w,min}$ = 0.92% and GOF = 2.68. Non-identifiable reflexes and reflexes caused by the Vaseline used to fixate the sample were marked with black stars.

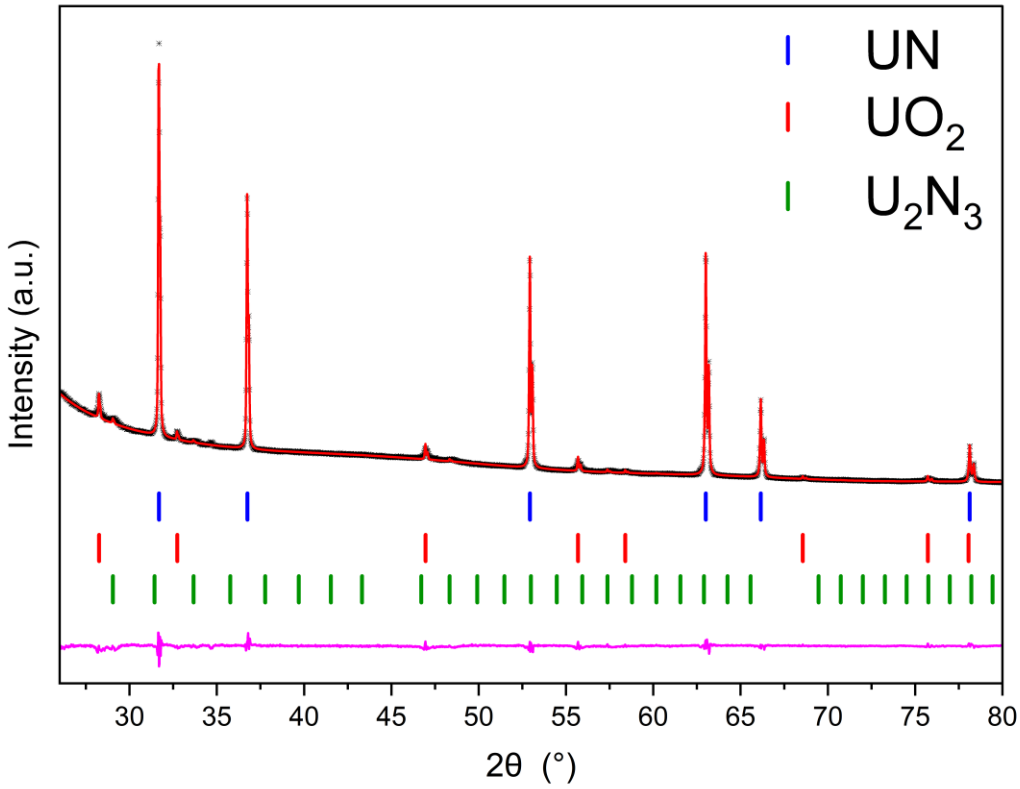

Figure S12. Rietveld profile of UN sample containing 6.4 wt% UO_2 and 1.2 wt% U_2N_3 used for XANES analysis. The black crosses, red and pink lines and vertical blue, red and violet markers respectively represent observed data, calculated profile, difference profile and allowed reflections of UN and UO_2 crystallising in cubic $Fm\bar{3}m$ structure with a = 4.890641(14) Å and a = 5.4718(1) Å, as well as U_2N_3 crystallising in $Ia\bar{3}$ structure with a = 10.648(1) Å. The fitting parameters are R = 1.81%, R_w = 2.51%, $R_{w\text{-}bkg}$ = 3.06%, $R_{w,min}$ = 1.01% and GOF = 2.50.

Supplementary Information Note 5 – Analysis of *Ln*N HERFD-XANES

Supplementary Figures S13, S14 and S15 as well as Supplementary Table S3 to illustrate and summarize the results of the high-resolution XANES analysis for DyN and PrN as well as their oxidized forms

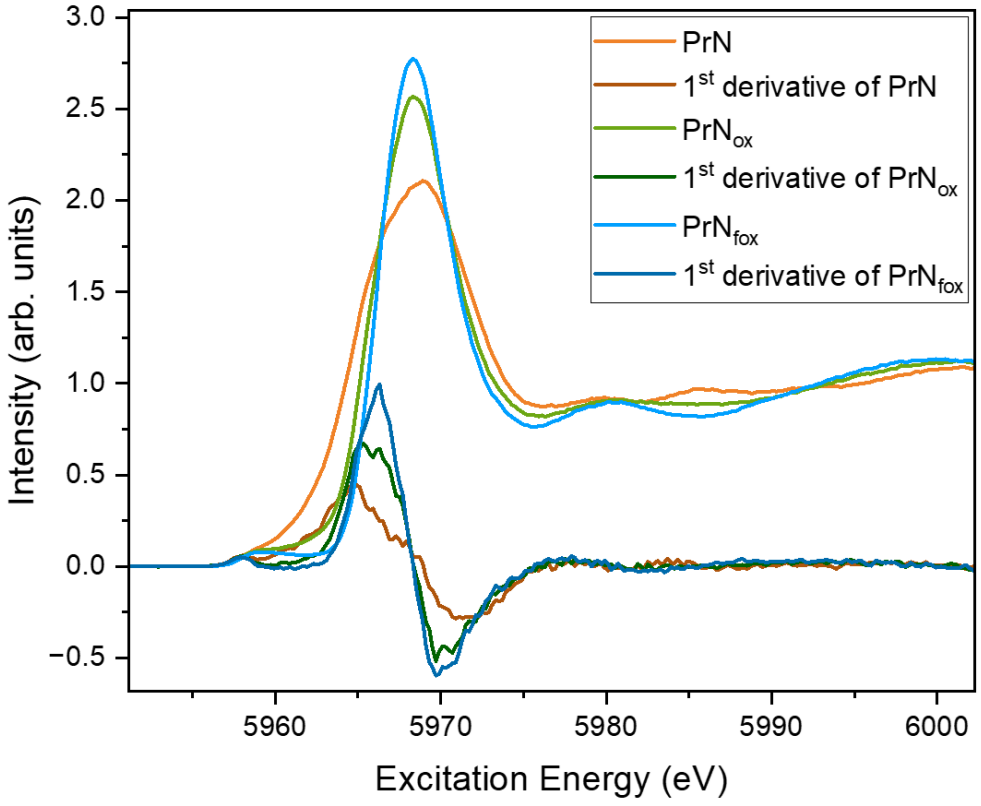

Figure S13. HR-XANES and their first derivatives for the Pr set of samples.

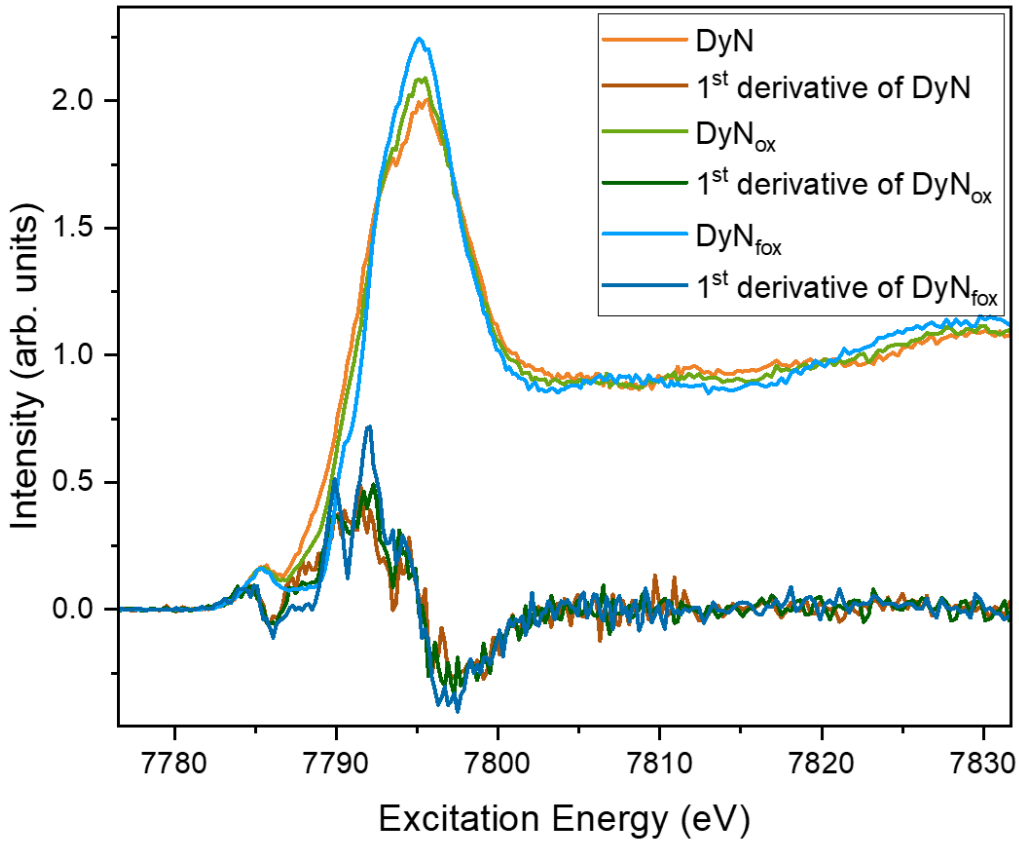

Figure S14. HR-XANES and their first derivatives for the Dy set of samples.

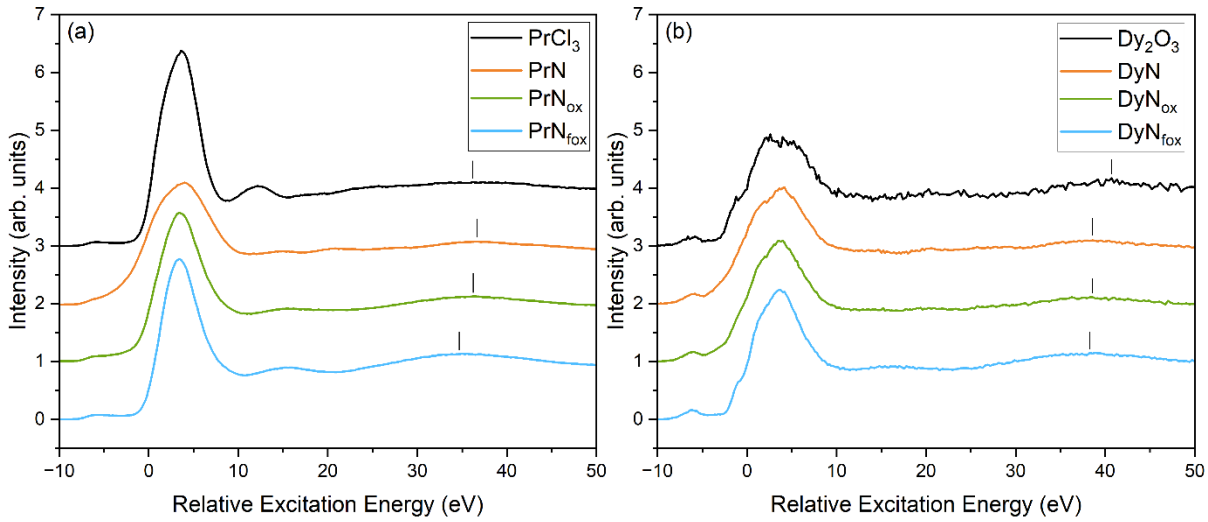

Figure S15. Vertically shifted HR-XANES of the Pr sample set (a) and the Dy sample set (b) on an excitation energy axis relative to the edge of the nitrides for better comparison of the change in spectral shape. The maxima of the post-edge peak are marked.

Table S3. Summary of pre-edge and edge positions, as well as their energetic differences.

Compound	Pre-edge maximum [eV]	Edge Position [eV]	ΔE(*5d,4f*) [eV]
PrN	5958.9	5964.9	6.0
PrN_{ox}	5958.9	5965.3	6.4
PrN_{fox}	5958.9	5966.3	7.4
DyN	7785.5	7791.5	6.0
DyN_{ox}	7785.5	7792.3	6.8
DyN_{fox}	7785.3	7792.1	6.8

Supplementary Information Note 6 – High temperature TGA-DSC

Supplementary Figure S16 to Figure S18 display the TGA- and DSC-curves received by coupled TGA-DSC oxidation of U/*Ln*N (*Ln* = Pr, Nd, Gd, Tb, Dy, Ho, Tm, Lu) in air at 900 °C. The supplementary Figures S19 to Figure S27 display the Rietveld profiles of the respective oxidation residues. Table S4 summarises the crystallographic data of the oxidised phases against their respective literature parameters.

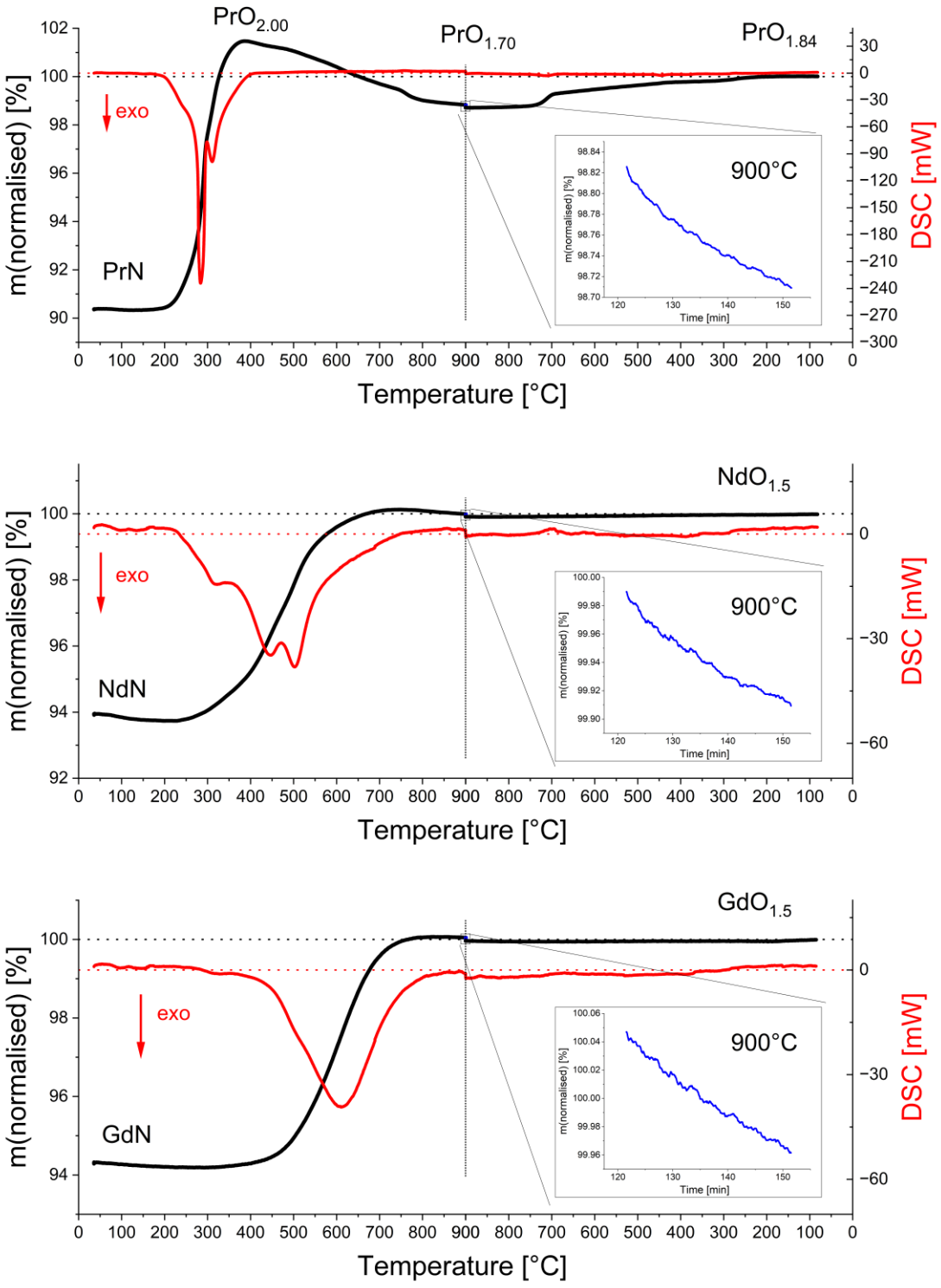

Figure S16. Combined heating and cooling black TGA- and red DSC curves of PrN, NdN and GdN heated to 900 °C in air with inset blue TGA curve of plateau performed at 900 °C.

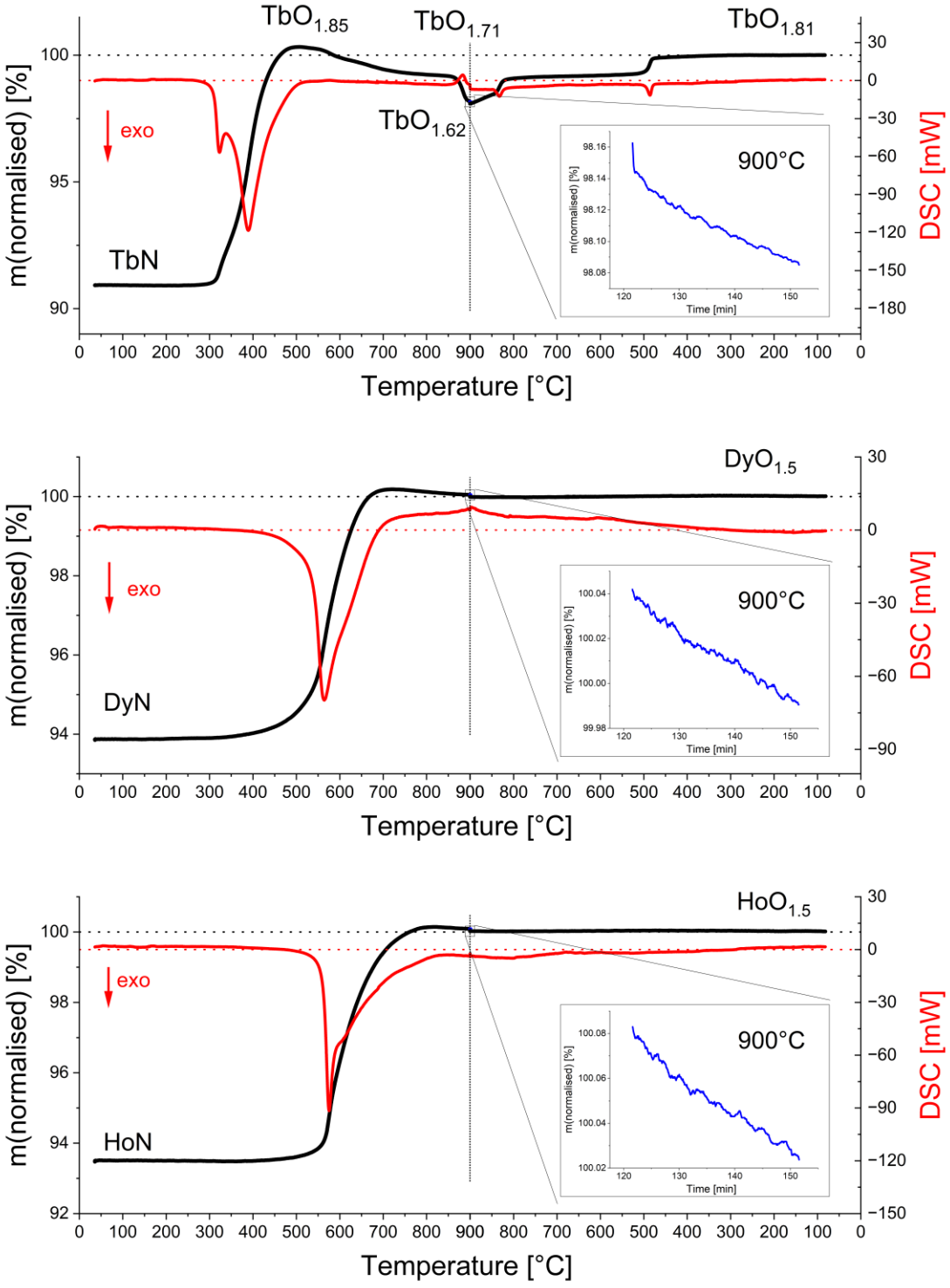

Figure S17. Combined heating and cooling black TGA- and red DSC curves of TbN, DyN and HoN heated to 900 °C in air with inset blue TGA curve of plateau performed at 900 °C.

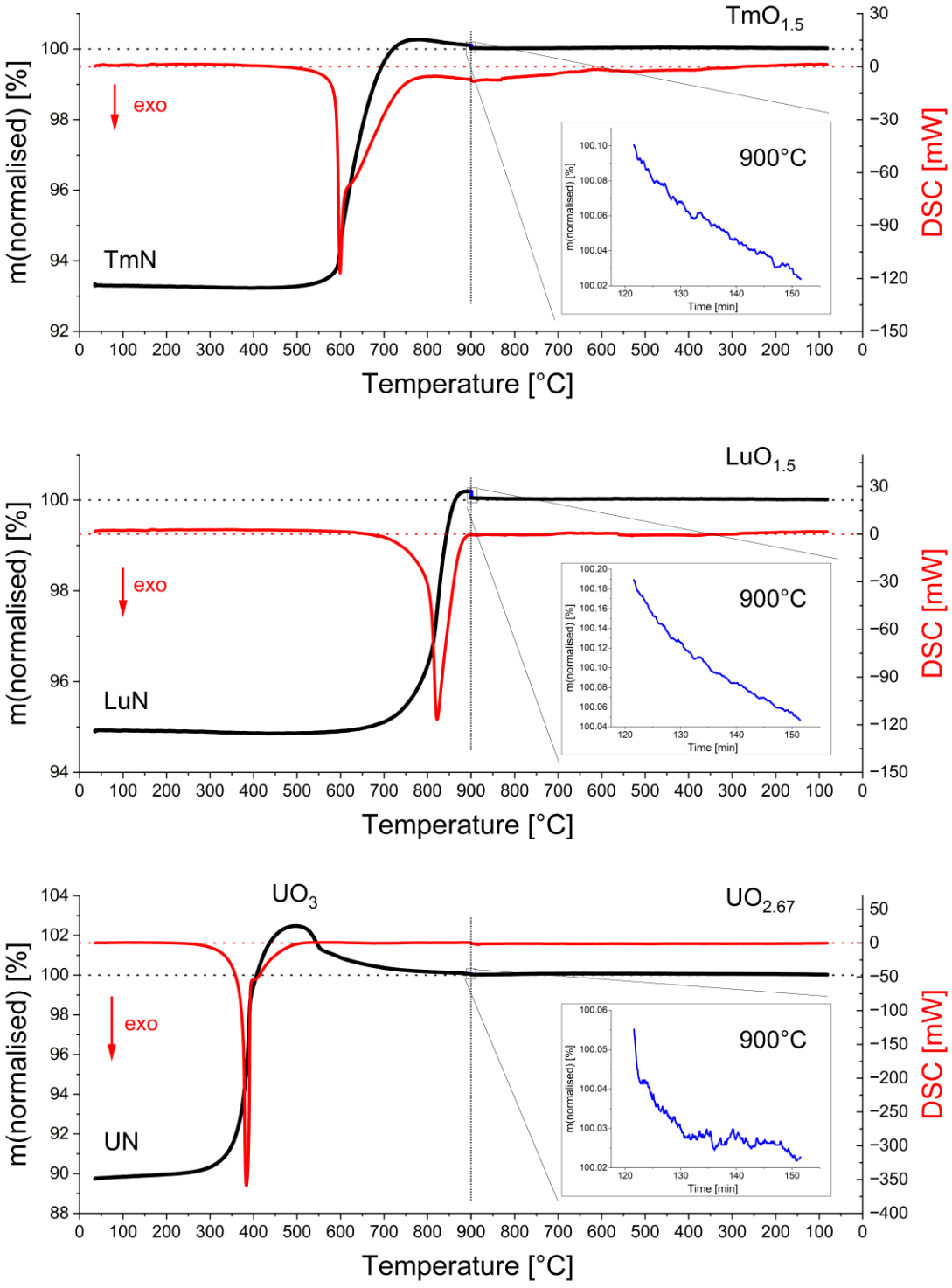

Figure S18. Combined heating and cooling black TGA- and red DSC curves of TmN, LuN and UN heated to 900 °C in air with inset blue TGA curve of plateau performed at 900 °C.

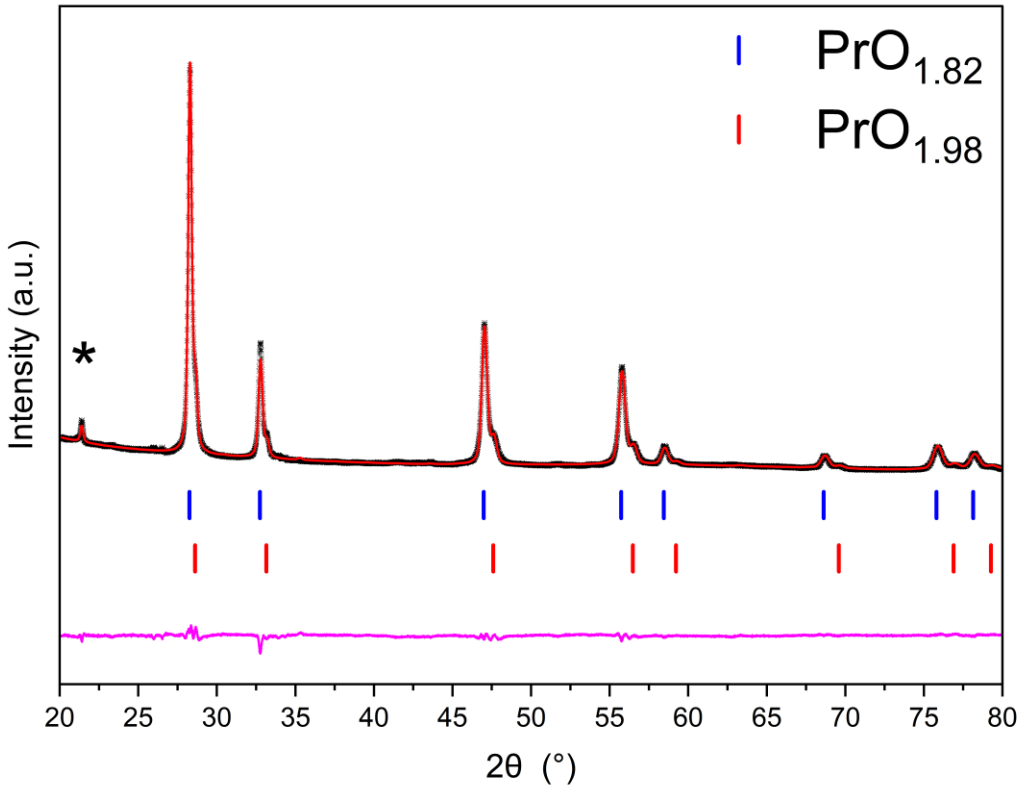

Figure S19. Rietveld profile of residues received when oxidising pristine PrN in air at 900 °C. The black crosses, red and pink lines and vertical blue, red and violet markers respectively represent observed data, calculated profile, difference profile and allowed reflections of $PrO_{1.82}$ and $PrO_{1.98}$ crystallising in cubic $Fm\bar{3}m$ structure. Non-identifiable reflexes and reflexes caused by the Vaseline used to fixate the sample were marked with black stars.

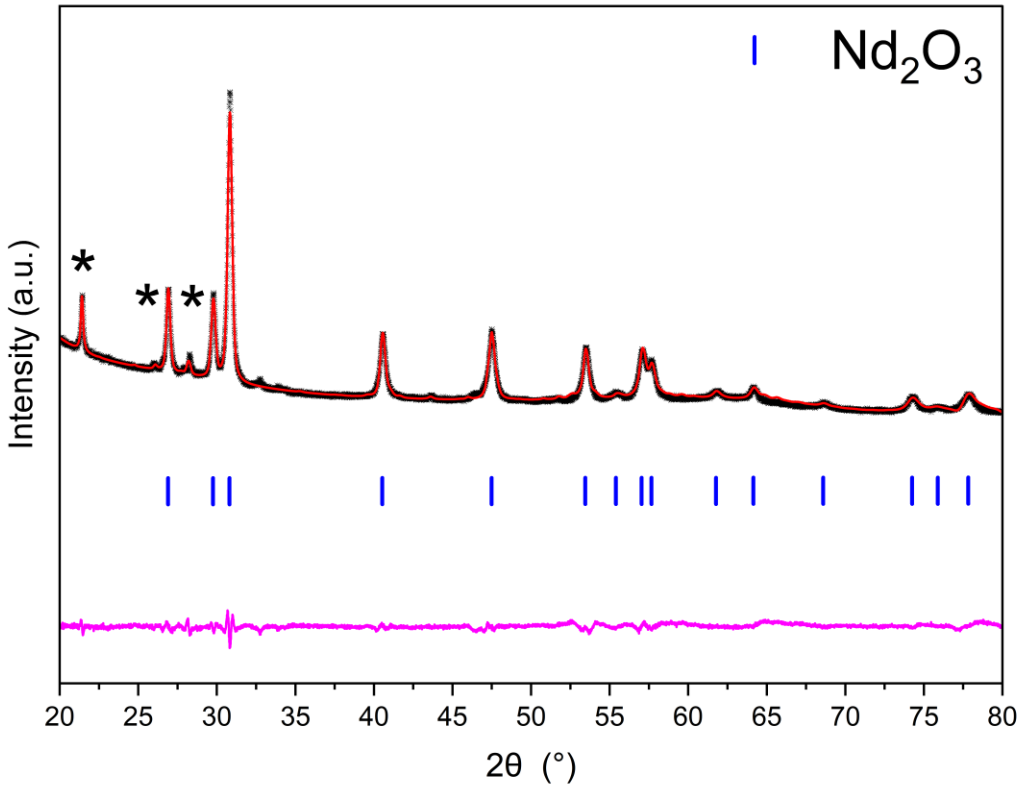

Figure S20. Rietveld profile of residues received when oxidising pristine NdN in air at 900 °C. The black crosses, red and pink lines and vertical blue, red and violet markers respectively represent observed data, calculated profile, difference profile and allowed reflections of Nd_2O_3 crystallising in hexagonal *P*63/*mmc* structure. Non-identifiable reflexes and reflexes caused by the Vaseline used to fixate the sample were marked with black stars.

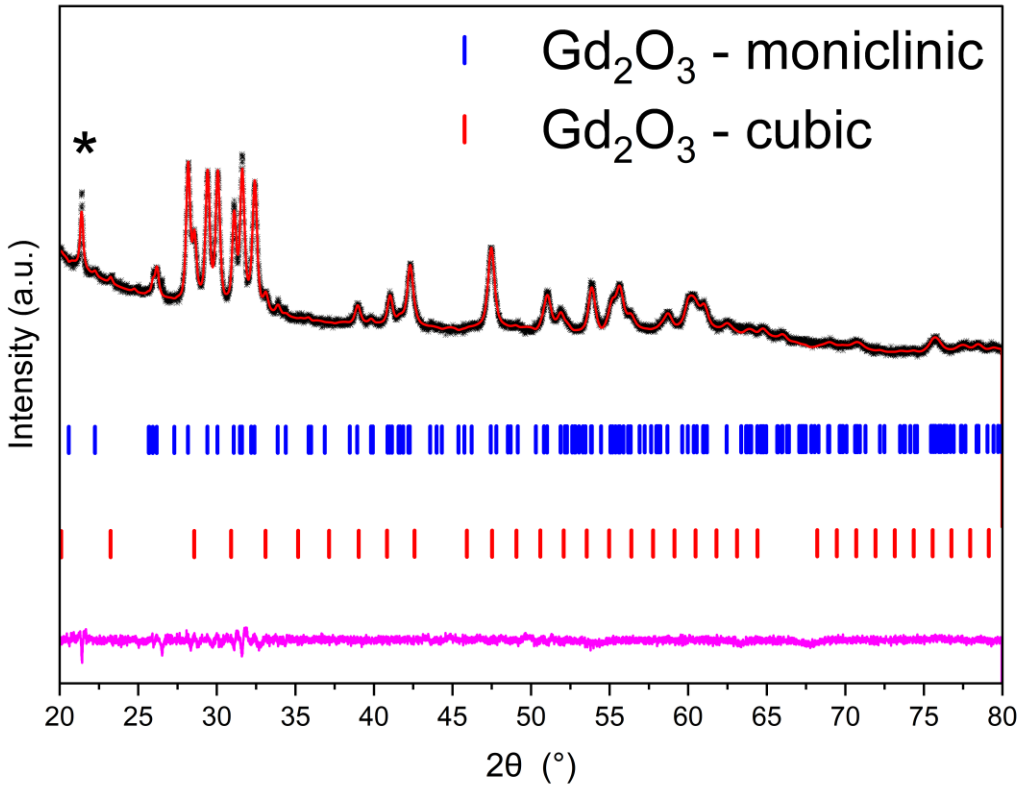

Figure S21. Rietveld profile of residues received when oxidising pristine GdN in air at 900 °C. The black crosses, red and pink lines and vertical blue, red and violet markers respectively represent observed data, calculated profile, difference profile and allowed reflections of Gd_2O_3 crystallising in monoclinic $C12/m1$ and cubic $Ia\bar{3}$ structure. Non-identifiable reflexes and reflexes caused by the Vaseline used to fixate the sample were marked with black stars.

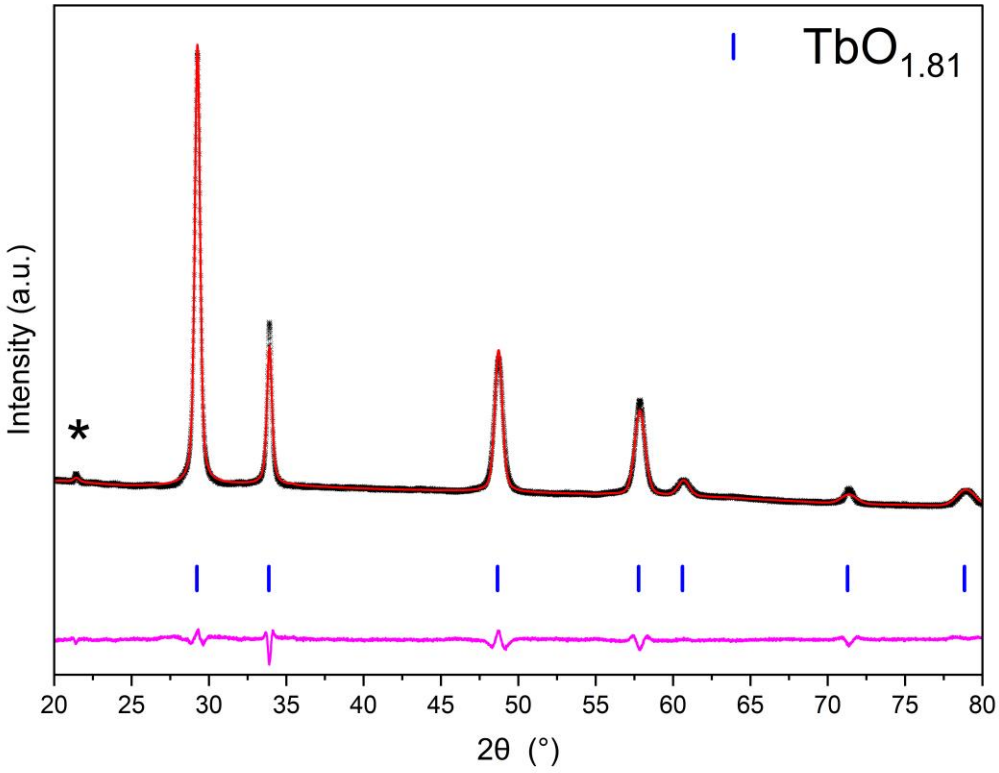

Figure S22. Rietveld profile of residues received when oxidising pristine TbN in air at 900 °C. The black crosses, red and pink lines and vertical blue, red and violet markers respectively represent observed data, calculated profile, difference profile and allowed reflections of $TbO_{1.81}$ crystallising in cubic $Fm\bar{3}m$ structure. Non-identifiable reflexes and reflexes caused by the Vaseline used to fixate the sample were marked with black stars.

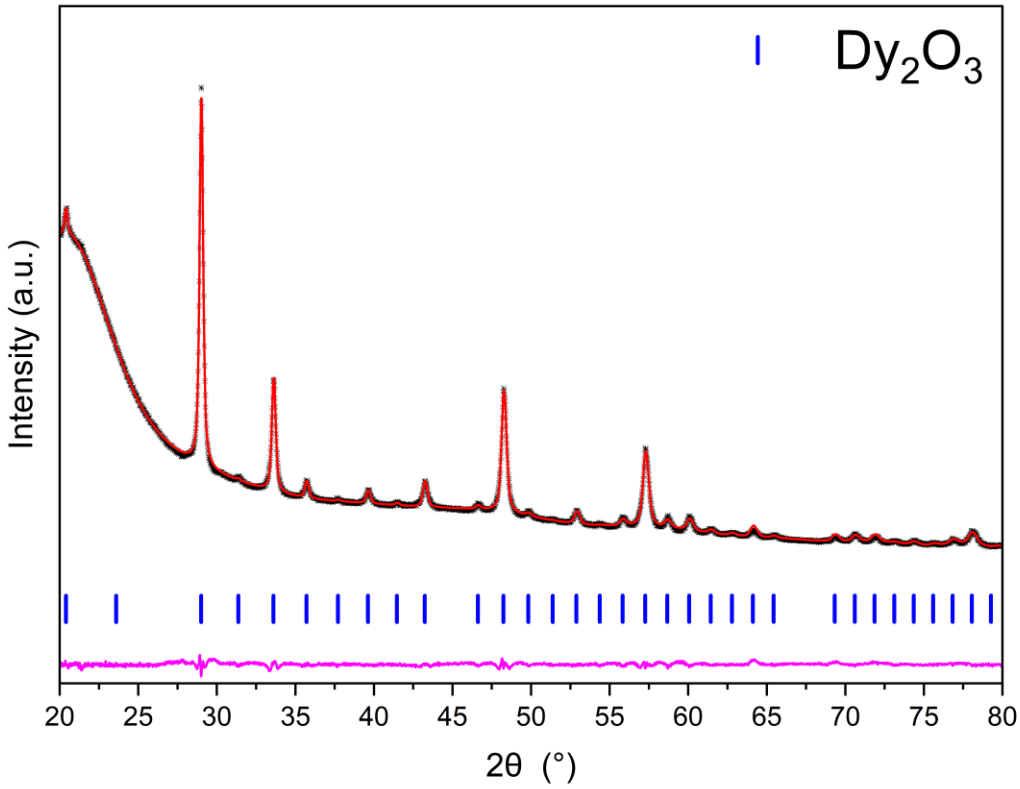

Figure S23. Rietveld profile of residues received when oxidising pristine DyN in air at 900 °C. The black crosses, red and pink lines and vertical blue, red and violet markers respectively represent observed data, calculated profile, difference profile and allowed reflections of Dy_2O_3 crystallising in cubic $Ia\bar{3}$ structure.

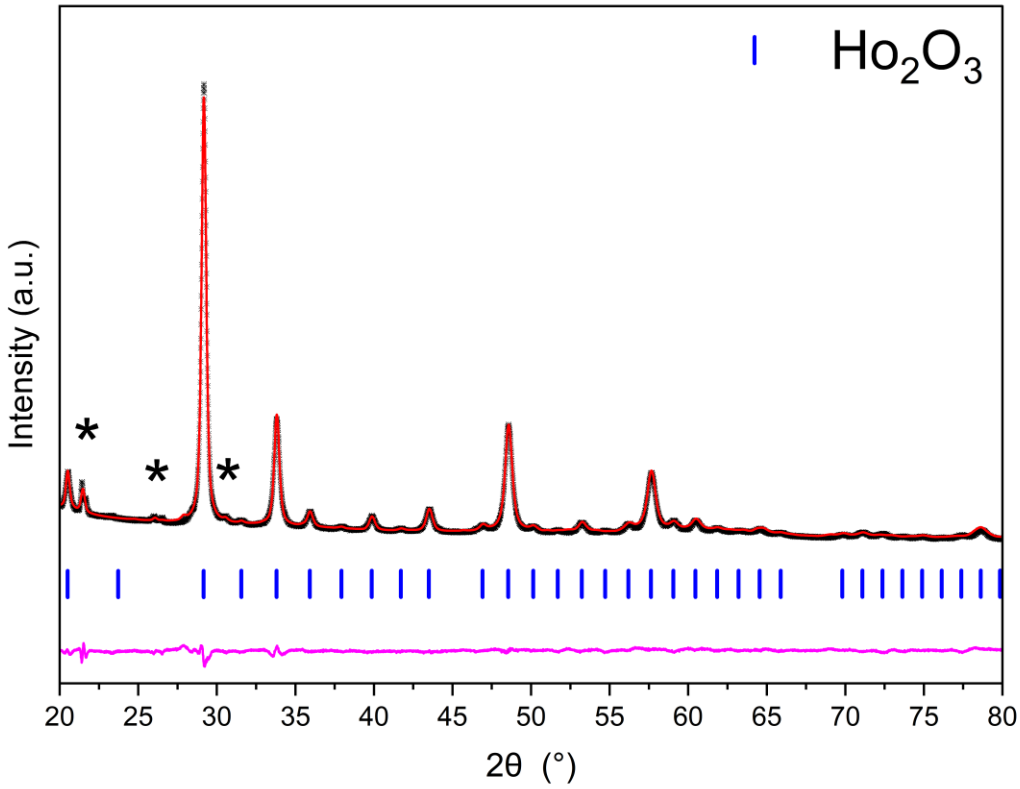

Figure S24. Rietveld profile of residues received when oxidising pristine HoN in air at 900 °C. The black crosses, red and pink lines and vertical blue, red and violet markers respectively represent observed data, calculated profile, difference profile and allowed reflections of Ho_2O_3 crystallising in cubic $Ia\bar{3}$ structure. Non-identifiable reflexes and reflexes caused by the Vaseline used to fixate the sample were marked with black stars.

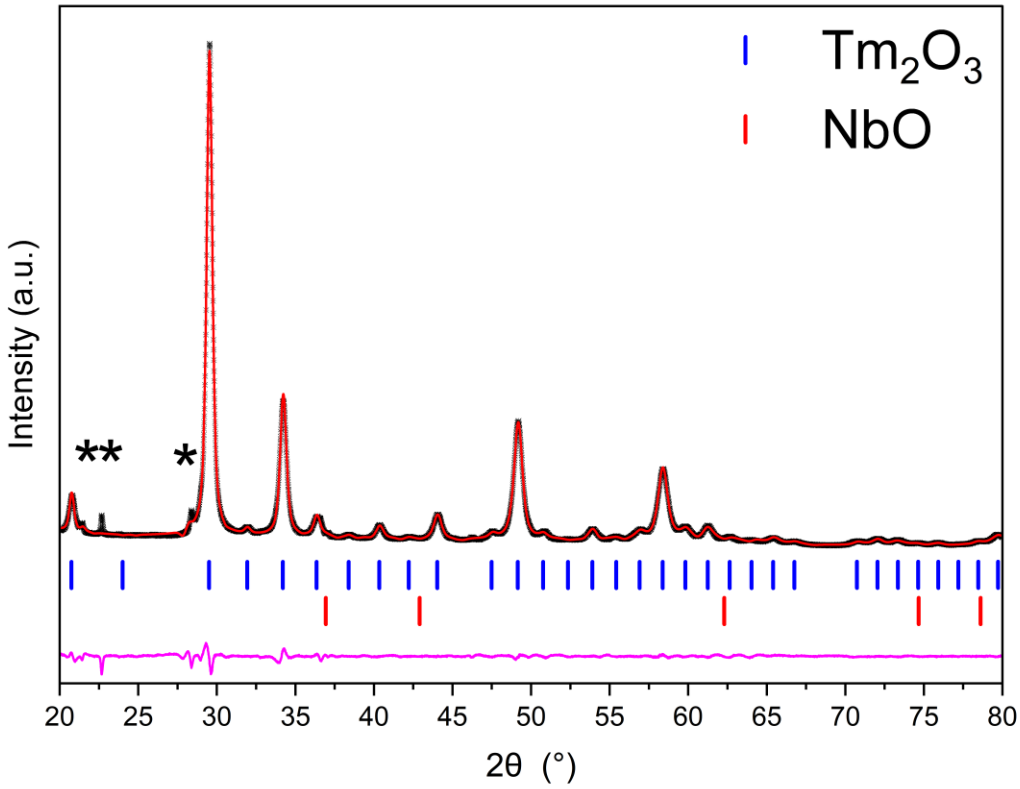

Figure S25. Rietveld profile of residues received when oxidising pristine TmN in air at 900 °C. The black crosses, red and pink lines and vertical blue, red and violet markers respectively represent observed data, calculated profile, difference profile and allowed reflections of Ho_2O_3 crystallising in cubic $Ia\bar{3}$ structure, as well as NbO resulting from NbN impurities in the pristine nitride. Non-identifiable reflexes and reflexes caused by the Vaseline used to fixate the sample were marked with black stars.

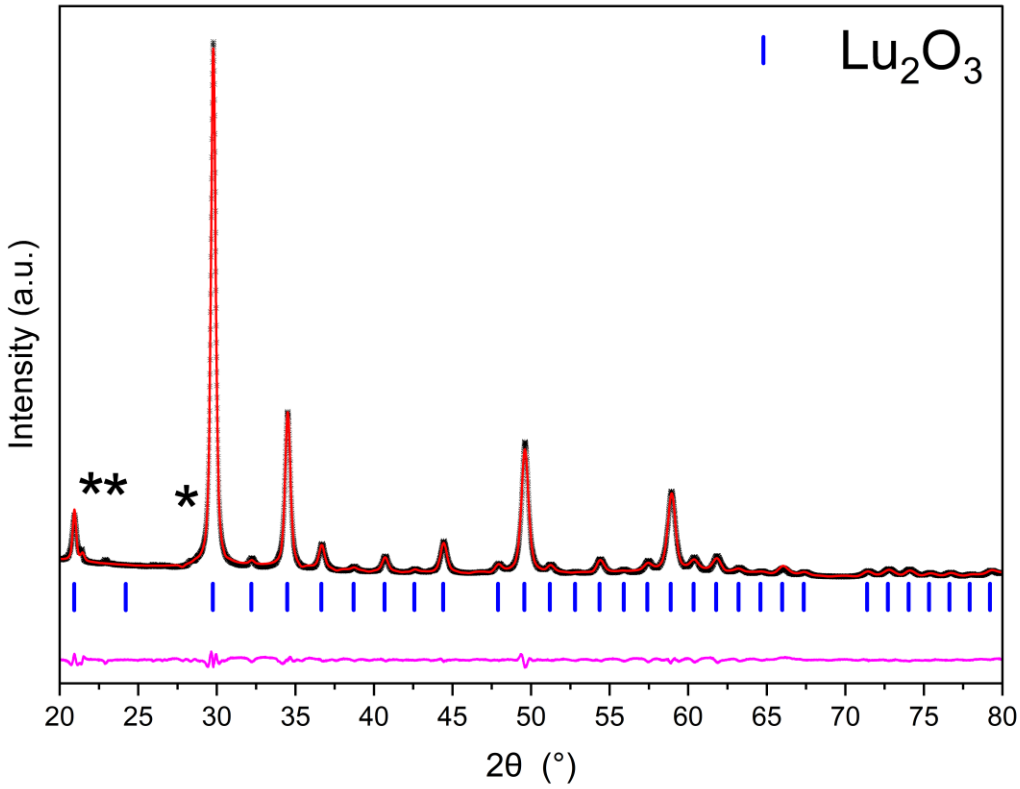

Figure S26. Rietveld profile of residues received when oxidising pristine LuN in air at 900 °C. The black crosses, red and pink lines and vertical blue, red and violet markers respectively represent observed data, calculated profile, difference profile and allowed reflections of Lu_2O_3 crystallising in cubic $Ia\bar{3}$ structure. Non-identifiable reflexes and reflexes caused by the Vaseline used to fixate the sample were marked with black stars.

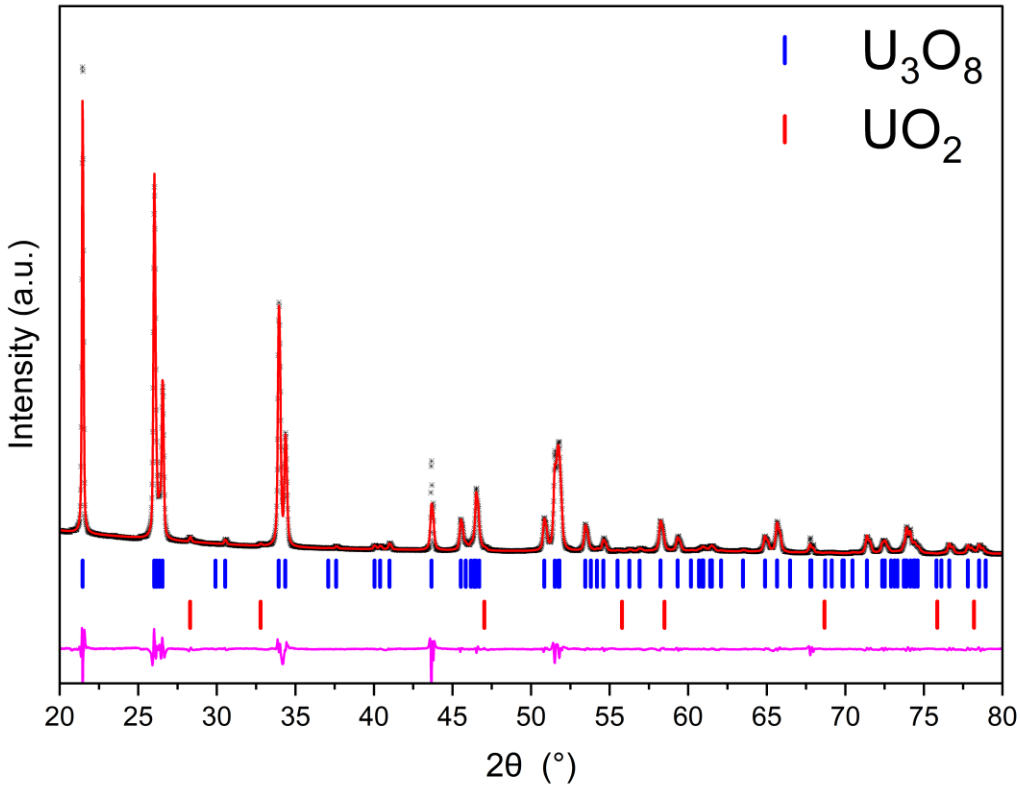

Figure S27. Rietveld profile of residues received when oxidising pristine UN in air at 900 °C. The black crosses, red and pink lines and vertical blue and red markers respectively represent observed data, calculated profile, difference profile and allowed reflections of U_3O_8 crystallising in orthorhombic *C*222 structure.

Table S4. Summary of determined crystalline phases arising from the oxidation of *Ln*N (*Ln* = Pr, Nd, Gd, Tb, Dy, Ho, Tm, Lu) in air at 900 °C via Rietveld analysis and their respective literature lattice parameters. Additional refinement results provided by the Rietveld software GSAS-II are shown in Supplementary Information Note 2, Table S2.

Compound	Oxidised Phase	Structure and Space Group	Lattice Parameters [Å]	Fitting factors	Literature lattice parameter [Å]
PrN	$PrO_{1.82}$	$Fm\bar{3}m$ (225)	a = 5.46601(8)	R = 2.32 % R_w = 3.02 %	a = 5.4602(1)
	$PrO_{1.98}$		a = 5.4003(3)		
NdN	Nd_2O_3	*P*63/*mmc* (194)	a = 3.8282(2) c = 6.0045(2)	R = 2.46 % R_w = 3.32 %	a = 3.8316(4) c = 6.0028(7) [1]
GdN	Gd_2O_3	*C*12/*m*1 (12)	a = 14.091(1) b = 3.5766(1) c = 8.7606(7) β = 100.222(4)	R = 1.00 % R_w = 1.37 %	a = 14.091(8) b = 3.5736(3) c = 8.761(6) β = 100.04 [2]
		$Ia\bar{3}$ (206)	a = 10.814(2)		a = 10.8139(2) [3]
TbN	$TbO_{1.81}$	$Fm\bar{3}m$ (225)	a = 5.28715(7)	R = 1.36 % R_w = 1.91 %	a = 5.286(3) [4]
DyN	Dy_2O_3	$Ia\bar{3}$ (206)	a =10.6675(3)	R = 0.87 % R_w = 1.18 %	a =10.6706(7) [5]
HoN	Ho_2N_3	$Ia\bar{3}$ (206)	a = 10.6001(2)	R = 3.06 % R_w = 3.81 %	a =10.606(2) [5]
TmN	Tm_2O_3	$Ia\bar{3}$ (206)	a =10.4775(1)	R = 3.04% R_w = 4.23 %	a =10.4480(6) [6]
LuN	Lu_2O_3	$Ia\bar{3}$ (206)	a = 10.3952(2)	R = 2.90 % R_w = 3.95 %	a = 10.3909(1) [7]
UN	U_3O_8	*C*222(21)	a = 6.7222(1) b = 11.9550(2) c = 4.14682(5)	R = 3.39 % R_w = 5.60 %	a = 6.704 b = 11.95 c = 4.142 [8]

References

1 Aldebert, P. & Traverse, J. P. Etude par diffraction neutronique des structures de haute temperature de La_2O_3 et Nd_2O_3. *Materials Research Bulletin* **14**, 303–323 (1979). https://doi.org:10.1016/0025-5408(79)90095-3

2 Ferguson, I. F. in *Acta Crystallographica Section A* Vol. 31 69.

3 Serebrennikova, P. S., Kudryavtsev, A. L., Naumov, N. G. & Gromilov, S. A. Gd_2O_3: Synthesis and X-ray diffraction analysis of single crystals, thermal expansion in the range of 90-490 K. *Journal of Structural Chemistry* **65**, 2429–2437 (2024). https://doi.org:10.1134/s0022476624120072

4 Guth, E. D. & Eyring, L. The terbium oxides. I. Dissociation pressure measurements: X-ray and differential thermal analyses 1. *Journal of the American Chemical Society* **76**, 5242–5244 (1954). https://doi.org:10.1021/ja01649a089

5 Maslen, E. N., Streltsov, V. A. & Ishizawa, N. A synchrotron X-ray study of the electron density in C -type rare earth oxides. *Acta Crystallographica Section B Structural Science* **52**, 414–422 (1996). https://doi.org:10.1107/s0108768195013371

6 Ishibashi, H., Shimomoto, K. & Nakahigashi, K. Electron density distribution and chemical bonding of Ln_2O_3 (*Ln* = Y, Tm, Yb) from powder X-ray diffraction data by the maximum-entropy method. *Journal of Physics and Chemistry of Solids* **55**, 809–814 (1994). https://doi.org:10.1016/0022-3697(94)90004-3

7 Pedroso, C. C. S., Carvalho, J. M., Rodrigues, L. C. V., Hölsä, J. & Brito, H. F. Rapid and energy-saving microwave-assisted solid-state synthesis of Pr^{3+}-, Eu^{3+}-, or Tb^{3+}-doped

Lu_2O_3 persistent luminescence materials. *ACS Applied Materials & Interfaces* **8**, 19593–19604 (2016). https://doi.org:10.1021/acsami.6b04683

8 Andresen, A. F. The structure of U_3O_8 determined by neutron diffraction. *Acta Crystallographica* **11**, 612–614 (1958). https://doi.org:10.1107/s0365110x5800164x